

Future Experimental Improvement for the Search of LNV Process in $e\mu$ Sector

Beomki Yeo,^{1,*} Yoshitaka Kuno,^{2,†} MyeongJae Lee,^{3,‡} and Kai Zuber^{4,§}

¹*Department of Physics, Korea Advanced Institute of Science and Technology (KAIST), Daejeon 34141, Republic of Korea*

²*Department of Physics, Graduate School of Science, Osaka University, Toyonaka, Osaka 560-0043, Japan*

³*Center for Axion and Precision Physics Research,*

Institute for Basic Science (IBS), Daejeon 34051, Republic of Korea

⁴*Institute for Nuclear and Particle Physics, Technische Universität Dresden, Germany*

(Dated: May 7, 2022)

Exploring the leptonic sector in frontier experiments is more of importance nowadays, since the conservation of lepton flavor and total lepton number are not guaranteed anymore in the Standard Model after the discovery of neutrino oscillations. $\mu^- + N(A, Z) \rightarrow e^+ + N(A, Z - 2)$ conversion in a muonic atom is one of the most promising channels to investigate the lepton number violation process, and the measurement of this process is planned in future $\mu^- - e^-$ conversion experiments with a muonic atom in a muon-stopping target. This paper discusses how to maximize the experimental sensitivity of the $\mu^- - e^+$ conversion by introducing the new requirement of the mass relation of $M(A, Z - 2) < M(A, Z - 1)$, where $M(A, Z)$ is the mass of the muon-stopping target nucleus, to get rid of the background from radiative muon capture. The sensitivity of the $\mu^- - e^+$ conversion is anticipated to have four orders of magnitude of improvement in forthcoming experiments using a proper target nucleus, which satisfies the mass relation. The most promising isotopes found are ^{40}Ca and ^{32}S .

PACS numbers: 13.35.Bv, 14.60.Ef, 36.10.Ee

I. INTRODUCTION

As lepton flavor violation was confirmed by the discovery of neutrino oscillation, much interest has moved to the whole leptonic sector in terms of the search for new physics beyond the Standard Model (SM). Anomalies in the leptonic sector governed by new physics have been explored within three major phenomena: (1) lepton universality violation (LUV), (2) charged lepton flavor violation (CLFV), (3) and lepton number violation (LNV). The SM, which preserves the lepton universality, expects that three generations of leptons behave consistently within the electroweak interaction. However, recent measurements of $\bar{B} \rightarrow D^{(*)}l^-\bar{\nu}_l$ [1–4] and $B^+ \rightarrow K^+l^+l^-$ [5] have shown non-trivial discrepancies (4σ and 2.6σ , respectively) to the SM predictions, showing the possibility of LUV in new physics [6]. An interesting implication of LUV is that CLFV phenomena in new physics may have sizable rates, which are observable in upcoming experiments [7, 8]. It is a remarkable aspect because, although the processes of CLFV can occur by neutrino mixing in the SM, the rates of the SM contributions were found to be extremely small, in the order of $\mathcal{O}(10^{-54})$ because of small neutrino masses. CLFV processes have been investigated in the past through the various muon decay channels: $\mu^- - e^-$ conversion, $\mu^+ \rightarrow e^+ + \gamma$ decay and

TABLE I. The experimental bounds (as 90% C.L.) of some selected LNV processes. (*) denotes the excited states of the daughter nucleus.

Process	Exp. bound	Ref
$0\nu\beta\beta$ (^{76}Ge)	Half-life $> 5.3 \times 10^{25}$ yr	[22]
$0\nu\beta\beta$ (^{136}Xe)	Half-life $> 1.07 \times 10^{26}$ yr	[23]
$\mu^- + \text{Ti} \rightarrow e^+ + \text{Ca}$	$\text{Br} < 1.7 \times 10^{-12}$	[17]
$\mu^- + \text{Ti} \rightarrow e^+ + \text{Ca}^*$	$\text{Br} < 3.6 \times 10^{-11}$	[17]
$K^+ \rightarrow \mu^+\mu^+\pi^-$	$\text{Br} < 8.6 \times 10^{-11}$	[20]

$\mu^+ \rightarrow e^+ + e^+ + e^-$ decay in the expectation of a discovery of new physics [9].

The observation of LNV would provide crucial clues on the small neutrino mass (\lesssim eV). The LNV processes, with the change of lepton number by two units ($\Delta L = 2$), can be mediated by Majorana neutrinos through type-1 seesaw mechanism or new particles appearing at a high energy scale ($>$ TeV). These phenomena have been examined mostly by $0\nu\beta\beta$ decay [10], which corresponds to the LNV process in the ee sector. LNV processes in other sectors also have been explored with muon-to-positron conversion $\mu^- + N(A, Z) \rightarrow e^+ + N(A, Z - 2)$ [11–17] and rare Kaon decays like $K^+ \rightarrow \mu^+\mu^+\pi^-$ [18–21], while their experimental bounds are way behind that of $0\nu\beta\beta$ decay, as shown in Table. I.

Nevertheless, the $\mu^- - e^+$ conversion is worth being investigated further for two reasons: (1) The $\mu^- - e^+$ conversion is able to be discovered if LNV process is more likely to occur in flavour off-diagonal sectors, e.g., $e\mu$ sector, as implied by recent studies [24, 25]. Several theories

* byeo@kaist.ac.kr

† kuno@phys.sci.osaka-u.ac.jp

‡ myeongjaelee@ibs.re.kr

§ zuber@physik.tu-dresden.de

beyond the SM of particle physics, such as the Majorana neutrino, the doubly charged singlet scalar model [26, 27], and the left-right symmetric model [28] have been suggested as feasible theories for the $\mu^- - e^+$ conversion. (2) Its experimental sensitivity can significantly increase with the future $\mu^- - e^-$ conversion experiments because the event signatures (e^\pm) of both physics processes can be easily distinguished by the charge identification. In the upcoming COMET and Mu2e experiments¹ [29–31], which are originally designed to search for the $\mu^- - e^-$ conversion with the sensitivity of $\mathcal{O}(10^{-16})$, a similar scale of the sensitivity for the $\mu^- - e^+$ conversion can be achieved. However, the improvement of $\mu^- - e^+$ conversion sensitivity may be considerably limited by the background from radiative muon capture (RMC) if an improper muon-stopping target nucleus is used. For example, as we will show later, the sensitivity improvement is less than a factor of ten in the usage of an aluminum stopping target, which is the baseline design of the COMET and Mu2e experiments. In this study, this kind of limitation was surmounted by selecting a proper muon-stopping target nucleus, which suppresses the RMC background and improves the sensitivity with four orders of magnitude over the current limit.

Nuclear physics as well as particle physics models comes into play since the $\mu^- - e^+$ conversion changes an atomic number of the nucleus by two units. In other words, the $\mu^- - e^+$ conversion is associated with nuclear interaction, which is represented as a nuclear matrix element in the calculation of the decay rate. Another aspect of nuclear interaction is that the nucleus in the final state after the $\mu^- - e^+$ conversion is divided into two cases in which a daughter nucleus stays in the ground state or enters excited states. The transition to the ground state of the daughter nucleus may not be dominating since the coherence of the nucleus, which in the $\mu^- - e^-$ conversion, is not expected in the $\mu^- - e^+$ conversion. Nevertheless, in this work, we focus on the case of the ground state since the excited states suffer more from background influence, and the momentum spectrum of signals for excited states is not known well due to the uncertainty of nuclear physics.

The remainder of this letter is organized as following: In Sec. II, we introduce the new requirement for the muon-stopping target nucleus with the mass of $M(A, Z)$ to suppress the background and find the candidates of target nucleus, which meets such requirement. In Sec. III, we estimate and compare the experimental sensitivities, i.e., the average upper limits, among the target nucleus candidates with simulation results. The summary follows in Sec. IV.

II. TARGET NUCLEUS CANDIDATES FOR THE $\mu^- - e^+$ CONVERSION

A. Mass relation of target nucleus

CLFV experiments based on a pulsed muon beam are performed as follows. A pulsed proton beam hits a pion production target to generate a bunch of pions. The negative pions are captured by a solenoidal magnetic field and are sent to a muon-stopping target, while most of the pions decay into muons during transport. These muons are stopped at the muon-stopping target, forming a muonic atom, and subsequently cascade down to the 1s ground state, followed either by muon decays in the 1s orbit of a muonic atom (decay-in-orbit=DIO), or by muon captures by a nucleus. If the $\mu^- - e^+$ conversion occurs, a single positron is emitted, and the measurement of the single positron is the signature of the process. The event measurement is made during the delayed time interval of the bunch period to avoid a huge background by a beam during the prompt interval of bunch period. For the transition to the ground state of the daughter nucleus, the signal positron is mono-energetic, and its energy ($E_{\mu^-e^+}$) is given by

$$E_{\mu^-e^+} = m_\mu + M(A, Z) - M(A, Z-2) - B_\mu - E_{recoil}, \quad (1)$$

where m_μ , B_μ , and E_{recoil} are the muon mass, the 1s binding energy of the muonic atom, and the recoil energy of the nucleus, respectively. Here, $M(A, Z)$ is the mass of the target nucleus, and $M(A, Z-2)$ is the mass of the ground state of the daughter nucleus. In the case of the $\mu^- - e^-$ conversion, the signal energy is $E_{\mu^-e^-} = m_\mu - B_\mu - E_{recoil}$, where the mass terms in the Eq. (1) are absent since the target and the daughter nuclei are the same.

There are two major sources of background in the $\mu^- - e^\pm$ detection: (1) DIO, and (2) RMC, as indicated by Ref. [12, 14–17]. DIO has an endpoint energy (E_{DIO}^{end}), the same as $E_{\mu^-e^-}$, and can emit a high energy e^- , which is an intrinsic background for the $\mu^- - e^-$ detection. It can also fake the signal in the $\mu^- - e^+$ detection when the charge is misidentified. But it is expected that the charge misidentification hardly occurs because of the high resolution of the tracking detectors. In case of RMC, the emitted γ can generate a high energy e^- or e^+ after an asymmetric pair production being an intrinsic background for both of the $\mu^- - e^\pm$ conversion. and its endpoint energy (E_{RMC}^{end}) is kinematically given by

$$E_{RMC}^{end} = m_\mu + M(A, Z) - M(A, Z-1) - B_\mu - E_{recoil}, \quad (2)$$

where $M(A, Z-1)$ is the mass of the daughter nucleus of RMC. The background from RMC can be negligible if the corresponding signal energy ($E_{\mu^-e^\pm}$) is higher than E_{RMC}^{end} . Since the simultaneous search for both conversions is desired, two mass relations between nuclei are required to avoid the RMC background: (1) $M(A, Z-2) < M(A, Z-1)$ for the $\mu^- - e^+$ conversion,

¹ Both of the COMET Phase-1 and the Mu2e experiments can measure the $\mu^- - e^+$ and $\mu^- - e^-$ conversion simultaneously, while the COMET Phase-2 experiment may need to change the polarity of the dipole magnetic field in the detector solenoid.

TABLE II. Stopping-target nucleus candidates whose $E_{\mu^-e^+}$ is higher than, or comparable to, E_{RMC}^{end} . If more than two isotopes satisfy the criteria, only one isotope with the highest natural abundance (N.A.) is listed. Nuclear masses required for the calculations are referred from AME2016 data [32]. Aluminum, which is the counterexample, is listed because it is considered the muon-stopping target nucleus in the upcoming CLFV experiments.

Atom	$E_{\mu^-e^+}$ (MeV)	$E_{\mu^-e^-}$ (MeV)	E_{RMC}^{end} (MeV)	N.A. (%)	f_{cap} (%)	τ_{μ^-} (ns)	A_T
²⁷ Al	92.30	104.97	101.34	100	61.0	864	0.191
³² S	101.80	104.76	102.03	95.0	75.0	555	0.142
⁴⁰ Ca	103.55	104.39	102.06	96.9	85.1	333	0.078
⁴⁸ Ti	98.89	104.18	99.17	73.7	85.3	329	0.076
⁵⁰ Cr	104.06	103.92	101.86	4.4	89.4	234	0.038
⁵⁴ Fe	103.30	103.65	101.93	5.9	90.9	206	0.027
⁵⁸ Ni	104.25	103.36	101.95	68.1	93.1	152	0.009
⁶⁴ Zn	103.10	103.04	101.43	48.3	93.0	159	0.011
⁷⁰ Ge	100.67	102.70	100.02	20.8	92.7	167	0.013

and (2) $M(A, Z) < M(A, Z - 1)$ for the $\mu^- - e^-$ conversion. The latter requirement is generally met for most of the stable nuclei, but the number of nuclei satisfying the former one is limited because the daughter nucleus of the $\mu^- - e^+$ conversion is usually less stable than that of RMC. However, such tendency can be reversed when even-even nuclei are used as the target material since the nucleons in the daughter nucleus of the $\mu^- - e^+$ conversion, which is an even-even nucleus again, can be more tightly bound due to the nuclear pairing force, whereas it is not the case for RMC with the odd-odd daughter nucleus. This kind of consideration is similar to the target selection in the $0\nu\beta\beta$ decay experiments which require the mass relations of $M(A, Z) > M(A, Z + 2)$ and $M(A, Z) < M(A, Z + 1)$ to enable the double beta decay, and forbid the single beta decay, respectively.

B. Search for the target nucleus candidates

Table II shows the list of candidate target nuclei with atomic mass ≤ 70 , which satisfy the requirements. Heavier nuclei were not considered due to their shorter lifetimes of muonic atoms, leading to lower efficiencies in the finite time window of measurements, as explained in the next paragraph. In the present calculation of each energy value, B_μ was obtained by assuming a point-like nucleus while this may not hold for heavier nuclei due to the larger size of the nucleus, and further corrections are required [33]. In Table II, E_{RMC}^{end} from Eq. (2) assumes RMC without an additional nucleon emission. RMC with nucleon emission can also generate backgrounds if its endpoint energy is higher than $E_{\mu^-e^+}$ or $E_{\mu^-e^-}$. However, this is not the problem in most cases because the binding energy per nucleon is around 7–9 MeV for the stable nuclei, which means that the endpoint energy gets lowered

by a similar amount.

There are other requirements from an experimental point of view. For instance, the muon capture rate (f_{cap}) and the muonic-atom lifetime (τ_{μ^-}) of each nucleus listed [34, 35] in Table II should be taken into account because f_{cap} is proportional to the number of signal events, and τ_{μ^-} is an important factor to determine the event acceptance in the time window of measurement (A_T). The values of A_T in Table II were calculated with a mathematical toy model. The followings are assumed: the bunch period (t_B) of the muon beam of 1 μ s, the timing window ($[t_1, t_2]$) from 700 ns to 1 μ s, and the uniform time distribution of muons in the muon beam during 100 ns. Then, A_T is $N_{\text{time}}/N_{\text{total}}$, where N_{total} is the number of stopped muons in the target with the single muon bunch, and N_{time} is the number of decayed muons during the timing window. N_{time} is given by $\sum_{n=1}^{\infty} \int_{t_1+t_B(n-1)}^{t_2+t_B(n-1)} N(t) dt$, where $N(t)$ is the muon exponential decay convoluted by the uniform time distribution of muons.

Natural abundance is another important characteristic in the target selection for two reasons. One is that the background from other isotopes can perturb the signal, and the other is that the signal itself can be dispersed into a broader spectrum as long as the natural abundance of the candidate isotope is not high enough. Considering these features, ³²S and ⁴⁰Ca can stand as most promising candidates because of their relatively high natural abundances and A_T , while the other candidate isotopes still can be considered by appropriate enrichment techniques.

III. EXPERIMENTAL SENSITIVITIES OF TARGET NUCLEUS CANDIDATES

In this section, the experimental sensitivities of target nucleus candidates are estimated assuming that the positron events only occur by the $\mu^- - e^+$ conversion and RMC. The number of accepted positrons from the $\mu^- - e^+$ conversions ($N_{\mu^-e^+}$) can be estimated by

$$N_{\mu^-e^+} \sim N_{\mu^-stop} \times f_{cap} \times \text{Br}(\mu^- - e^+) \times \mathcal{E}, \quad (3)$$

where N_{μ^-stop} is the total number of the stopped muons in the target, $\text{Br}(\mu^- - e^+)$ is the branching ratio of the $\mu^- - e^+$ conversion, in which daughter nucleus stays in the ground state, and \mathcal{E} is the net acceptance of signal positrons in the detector. \mathcal{E} is assumed to be the same for the $\mu^- - e^+$ conversion and RMC positrons.

The energy spectrum of RMC photons can be represented by [36]

$$P(x) \simeq C(1 - 2x + 2x^2)x(1 - x)^2, \quad x = \frac{E_\gamma}{E_\gamma^{end}}, \quad (4)$$

where the normalization constant C can be determined based on the results of previous experiments [37–39], and E_γ^{end} is the endpoint energy of RMC photons. In each experiment, the experimental values of E_γ^{end} were obtained by fitting the photon energy distribution with the

shape of Eq. (4). Those fitted spectra used to have an experimental value of E_{γ}^{end} around 10 MeV smaller than the theoretical endpoint energy, which is calculated based on kinematics. Regarding this discrepancy, Eq. (4) was actually developed from the closure approximation, in which the excitation energy of a nucleus is averaged into a single energy. There have been theoretical attempts to make a correction to this spectrum assuming that the final nuclei are excited with dipole resonance or higher resonance modes within the nuclear collective model [40, 41]. However, because there still remains an uncertainty in the nuclear excitation model, we utilize Eq. (4) with the kinematical endpoint energy (for example, 101.85 MeV for aluminum) for conservative estimation.

The number of accepted background positrons from RMC (N_{RMC}) above the low end of the energy window for signal positrons (E_{min}), is given by

$$N_{RMC} \sim N_{\mu^{-}stop} \times \text{Br}(\text{RMC}) \times P_{\gamma \rightarrow e^{-}+e^{+}} \times P_{V_{CT}} \times P_{E_{e^{+}} > E_{min}} \times \mathcal{E}, \quad (5)$$

where $\text{Br}(\text{RMC})$ is the branching ratio of RMC whose photon energy is higher than E_{min} , $P_{\gamma \rightarrow e^{-}+e^{+}}$ is the probability of a pair production, $P_{V_{CT}}$ is the probability that a pair production vertex is located inside the stopping target, and $P_{E_{e^{+}} > E_{min}}$ is the probability that a positron from the pair production has an energy higher than E_{min} . Here, $P_{V_{CT}}$ is included because the events that the vertex of pair production is located outside the stopping target can be avoided by using extrapolation of the positron tracks. There is another probability that internal conversion could occur with an off-shell photon. Since there have not been detailed studies on the energy spectrum of positrons emitted by the internal conversion, the amount of background was conservatively assumed to be the same as the on-shell RMC background throughout this paper.

In the following subsections, simulation studies using Geant4 [42] are shown, which were carried out with the muon-stopping target made of aluminum and target nucleus candidates in Table. II, respectively.

A. Subcase: aluminum target

For the sensitivity estimation, it is required to know the probability density functions (PDF) of positrons from both of the $\mu^{-} - e^{+}$ conversion and RMC, including their normalization factors of PDF, i.e., $N_{\mu^{-}e^{+}}$ and N_{RMC} . The PDF of signal positrons was obtained by generating 10^4 positrons with the energy of $E_{\mu^{-}e^{+}}$ in the aluminum muon-stopping target. The muon-stopping target was composed of 17 flat disks whose radius is 100 mm, thickness is 200 μm , and the spacing between disks is 50 mm, which benchmarked the design of the COMET target [29]. The energy of positrons was measured after they get out of the target to consider the energy loss in the target. The PDF of $f(E_{\mu^{-}e^{+}} - x)$, where $f(x)$ is the standard Landau distribution, was used to fit the

signal positron distribution. The fitted PDF was normalized to $N_{\mu^{-}e^{+}}$, which is determined by the value of $\text{Br}(\mu^{-} - e^{+})$, while $N_{\mu^{-}stop}$ of 10^{18} and \mathcal{E} of 10^{-2} were chosen to achieve the $\mu^{-} - e^{-}$ conversion sensitivity of $\mathcal{O}(10^{-16})$ with the aluminum target, based on the specifications of the upcoming experiments [29–31].

N_{RMC} was obtained by generating 10^7 photons with the RMC spectrum above 90.30 MeV (E_{min}) inside the aluminum stopping targets. Simulation results showed that $P_{\gamma \rightarrow e^{-}+e^{+}}$ is 0.97, $P_{V_{CT}}$ is 0.0058, and $P_{E_{e^{+}} > E_{min}}$ is 0.018. $\text{Br}(\text{RMC})$ has the value of 6.22×10^{-7} in the energy range from 90.30 MeV to 101.85 MeV according to the result of Ref. [34]. By plugging these values into Eq. (5), N_{RMC} is expected to be 6.24×10^5 without considering the internal conversions of the off-shell photons. For the PDF of RMC positrons, another simulation was done independently to get enough samples of positrons from RMC. The RMC photons of 2×10^6 with the same energy range were generated inside the large size of aluminum, in which almost half of photons decay via pair productions. The PDF of positrons from the pair production was fitted to the power function of $A(E_{RMC}^{end} - x)^y$, where A is the normalization constant, x is the positron energy, and y is the fitted power of the function. The fitted PDF was forced to be zero above E_{RMC}^{end} , and convoluted by the Landau energy loss distribution $f(-x)$ of the signal positrons, assuming that energy loss distributions of positrons from $\mu^{-} - e^{+}$ and RMC would not be so different from each other. The convoluted PDF was normalized to N_{RMC} afterwards.

For an illustrative purpose, Fig. 1 shows the estimation of the energy spectrum of the RMC background from on-shell photons and the $\mu^{-} - e^{+}$ signal positron with a $\text{Br}(\mu^{-} - e^{+})$ of 1.7×10^{-12} , which is the current limit. The energy distributions of signal and RMC were convoluted with a Gaussian detector response function with 200 keV standard deviation. To estimate how much the sensitivity would be improved over the current limit, the statistical significance of the signal with a given $\text{Br}(\mu^{-} - e^{+})$ was examined using a maximum likelihood method. The systematical uncertainties were assumed to be negligible. With that assumption, $\text{Br}(\mu^{-} - e^{+})$, which has 3σ significance under the null hypothesis, was found to be 2.5×10^{-13} . When the internal conversions of RMC are included, $\text{Br}(\mu^{-} - e^{+}) < 3.5 \times 10^{-13}$ was found to have 3σ significance. These results imply that the sensitivity improvement of more than a factor of ten, which is $\text{Br}(\mu^{-} - e^{+}) < 1.7 \times 10^{-13}$, may not be achieved with aluminum.

B. Target of the candidate nuclei

The same simulation and analysis for the target nucleus candidates in Table II were done with the corresponding $E_{\mu^{-}e^{+}}$ and E_{RMC}^{end} . Since the RMC branching ratios of ^{32}S , ^{50}Cr , ^{64}Zn and ^{70}Ge have not been measured, we used the known branching ratios of nuclei in

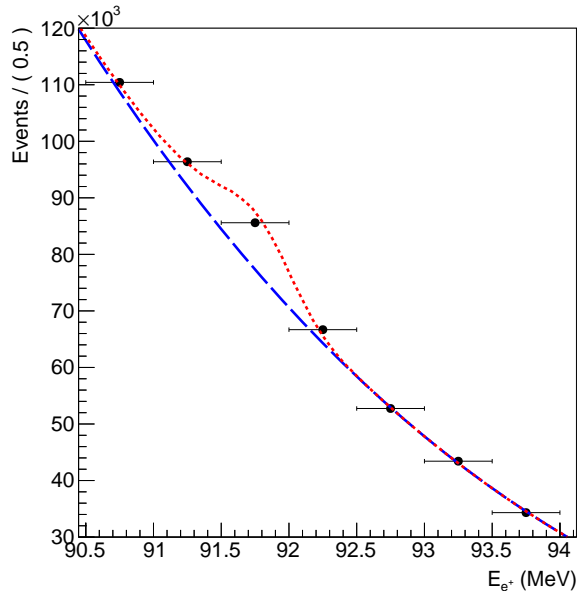


FIG. 1. Fitted energy distribution of the $\mu^- - e^+$ signal (short dashed red line) stacked on the on-shell RMC photon background (long dashed blue line) from ^{27}Al muon-stopping target when $\text{Br}(\mu^- - e^+) = 1.7 \times 10^{-12}$ and $N_{\mu^- \text{stop}} = 10^{18}$. Black dots are pseudo data of positrons generated by the background and signal composite model.

Ref. [34], whose atomic number is closest to the relevant nucleus, i.e., ^{28}Si for ^{32}S , Ti for ^{50}Cr , and ^{58}Ni for ^{64}Zn and ^{70}Ge . In the simulation, we assumed the target is made out of a pure isotope candidate. \mathcal{E} was normalized relative to that of aluminum (10^{-2}) by considering A_T and the signal acceptance in the energy window, A_E , that the positron energy is in an acceptable energy range defined more strictly to count the number of events accurately. In other words, $\mathcal{E} \rightarrow \mathcal{E} \times A_E/A_E^{\text{Al}} \times A_T/A_T^{\text{Al}}$, where A_E^{Al} and A_T^{Al} are A_E and A_T of aluminum, respectively. It should also be noted that the values of A_E for Eq. (3) and Eq. (5) are different from each other because of the difference in the two PDFs.

Since the numbers of the RMC background events for these candidate targets are much less than the aluminum case, the experimental sensitivities were estimated as the upper limit of 90% confidence level for a direct comparison with the current experimental upper limit of 1.7×10^{-12} (90% C.L.). The number of observed events (n) follows a Poisson distribution given by $p(n|s) = (s + b)^n e^{-(s+b)}/n!$, where s and b are the expected numbers of events of signal and background, which are equivalent to $N_{\mu^- e^+}$ and N_{RMC} , respectively. The experimental sensitivity with a confidence level (α), defined as the average upper limit of repeated experiments with no true signal, is given by the following equa-

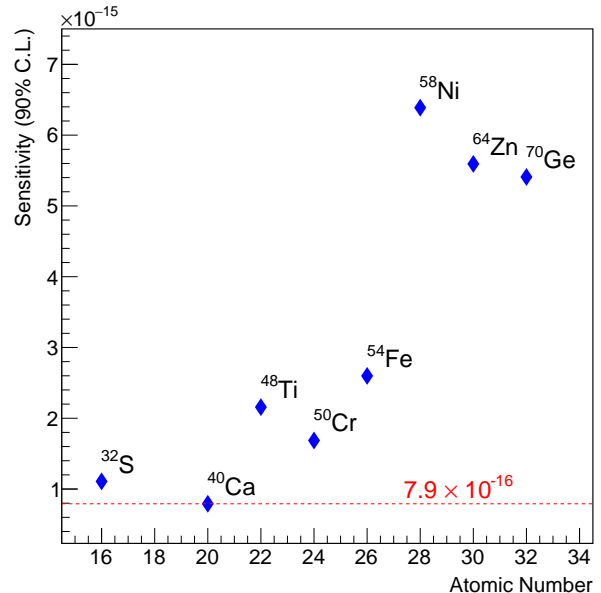


FIG. 2. Experimental sensitivities (90% C.L.) of the target nucleus candidates.

tion:

$$\frac{\int_0^{s_{up}} p(n = b|s) ds}{\int_0^{\infty} p(n = b|s) ds} = \alpha, \quad (6)$$

where s_{up} is the upper limit of the expected number of the signal events, which can be converted into the upper limit of the branching ratio from Eq. (3). The upper limit for each target nucleus was optimized by tuning the signal energy window (A_E) because both of $N_{\mu^- e^+}$ and N_{RMC} are dependent on A_E . Figure 2 shows the experimental sensitivity (90% C.L.) of each target nucleus, when the internal conversion of RMC background is included as well. As a result, ^{40}Ca showed the best experimental sensitivity of 7.9×10^{-16} among the candidates investigated, followed by ^{32}S with the sensitivity of 1.1×10^{-15} . The energy distributions of positrons from each nucleus are shown in Fig. 3 and Fig. 4, in which the branching ratio of the $\mu^- - e^+$ conversion is set to 1.0×10^{-14} , and $N_{\mu^- \text{stop}}$ is set to 10^{18} as the aluminum case.

IV. SUMMARY

A profound understanding of leptons is of importance because the fundamental conservation laws of leptons within the SM are easily violated in most of the theoretical models beyond the SM. Among them, LNV processes are important tools to reveal the mechanism of the neutrino mass generation. Investigation on the LNV processes have been mostly conducted by the $0\nu\beta\beta$ decay experiments, but the experimental search for the $\mu^- - e^+$ conversion can also be carried out as a complementary

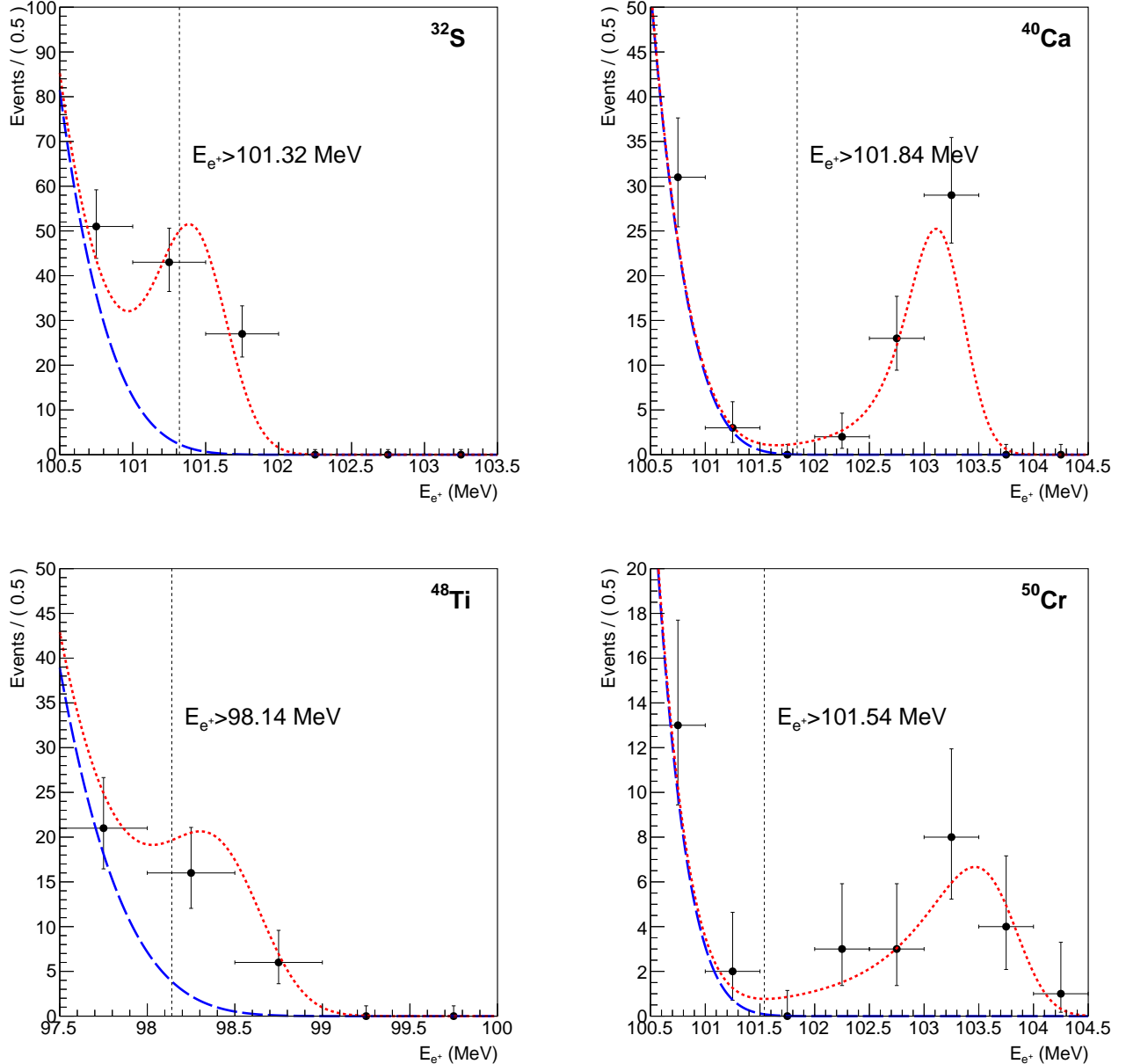


FIG. 3. Fitted energy distributions of the $\mu^- - e^+$ signal (short dashed red line) stacked on the RMC photon background (long dashed blue line) from ^{32}S , ^{40}Ca , ^{48}Ti , and ^{50}Cr muon-stopping target when $\text{Br}(\mu^- - e^+) = 1.0 \times 10^{-14}$ and $N_{\mu\text{-stop}} = 10^{18}$. The inequality beside the vertical black dotted line represents the signal energy window, and the line corresponds to its lower boundary. Black dots are pseudo data of positrons generated by the background and signal composite model.

channel to the $0\nu\beta\beta$ decay. Since a great leap of the sensitivity of the $\mu^- - e^+$ conversion is expected with the future CLFV experiments, it is essential to make a full exploration of the current experimental scheme.

For this purpose, we introduced new requirement of the target nucleus mass of $M(A, Z)$ satisfying $M(A, Z - 2) < M(A, Z - 1)$ to suppress the backgrounds from RMC. Several appropriate target candidates of even-even nuclei were found to meet the criteria. We estimated the experimental sensitivities of such target nuclei candidates

in a general experimental set-up. In conclusion, calcium (^{40}Ca) and sulfur (^{32}S) have the best experimental sensitivities about $\mathcal{O}(10^{-16})$ in the $\mu^- - e^+$ conversion detection, which results in the four orders of magnitude of improvement compared to the current upper limit. Another advantage of these two materials is that they will also have better sensitivities in the $\mu^- - e^-$ conversion measurement due to their relatively high timing efficiencies. It should be noted that the actual sensitivity would be different in the real experiment because some factors

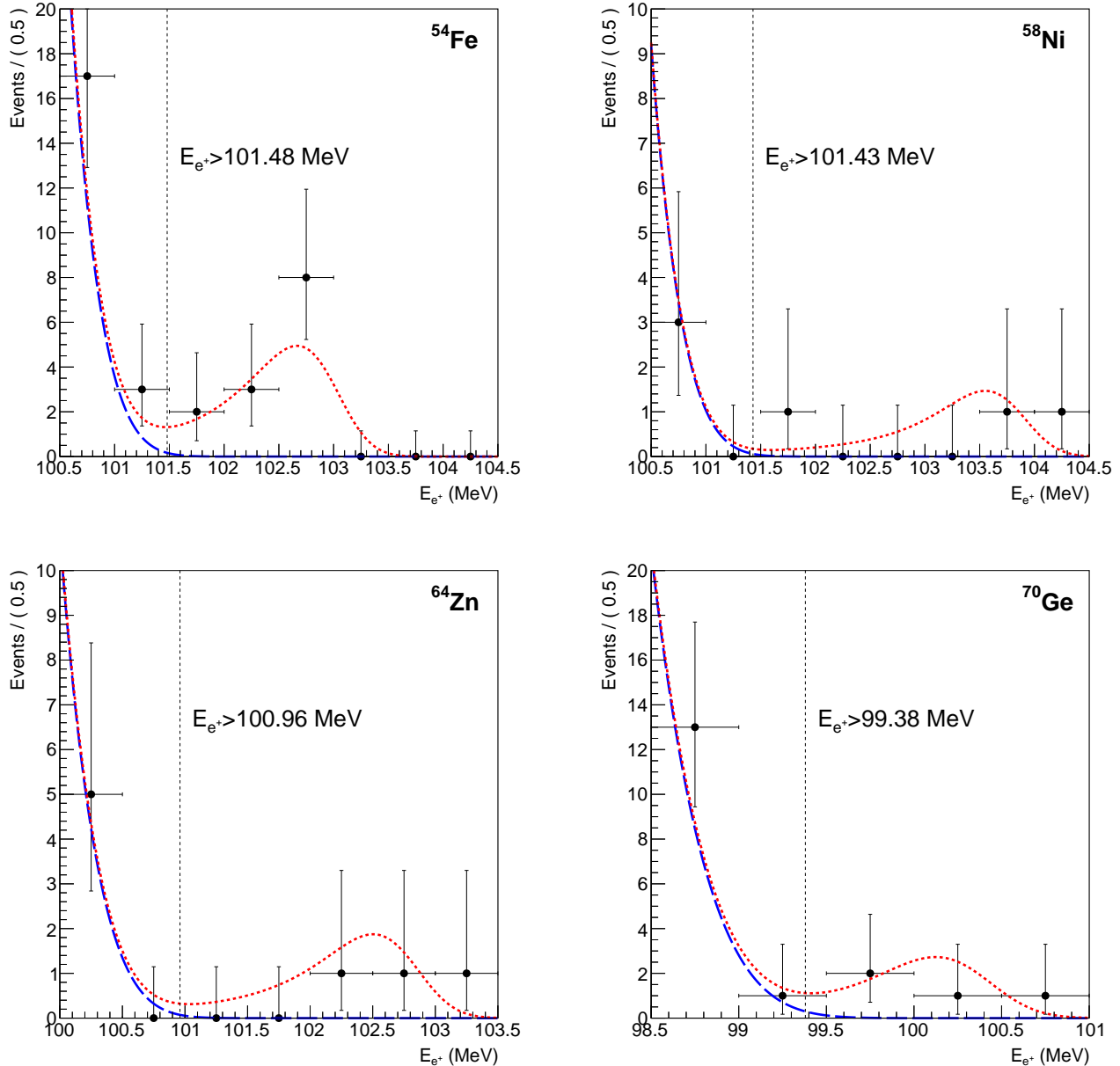


FIG. 4. Fitted energy distributions of the $\mu^- - e^+$ signal (short dashed red line) stacked on the RMC photon background (long dashed blue line) from ^{54}Fe , ^{58}Ni , ^{64}Zn , and ^{70}Ge muon-stopping target when $\text{Br}(\mu^- - e^+) = 1.0 \times 10^{-14}$ and $N_{\mu\text{-stop}} = 10^{18}$. The inequality beside the vertical black dotted line represents the signal energy window, and the line corresponds to its lower boundary. Black dots are pseudo data of positrons generated by the background and signal composite model.

such as systematical uncertainties are not considered in this paper. But this result can be a useful standard in the selection of the muon-stopping target material in future experiments.

ACKNOWLEDGMENTS

This work of B.Y. and M.L. was supported by the Institute for Basic Science of Republic of Korea (project

number: IBS-R017-D1-2017-a00). This work of Y.K. was supported in part by the Japan Society of the Promotion of Science (JSPS) KAKENHI Grant No. 25000004. We would like to thank the National Institute of Nuclear and Particle Physics (IN2P3) for providing the computing resources.

-
- [1] J. P. Lees *et al.* (The BABAR Collaboration), Phys. Rev. D **88**, 072012 (2013).
- [2] M. Huschle *et al.* (Belle Collaboration), Phys. Rev. D **92**, 072014 (2015).
- [3] Y. Sato *et al.* (Belle Collaboration), Phys. Rev. D **94**, 072007 (2016).
- [4] R. Aaij *et al.* (LHCb Collaboration), Phys. Rev. Lett. **115**, 111803 (2015).
- [5] R. Aaij *et al.* (LHCb Collaboration), Phys. Rev. Lett. **113**, 151601 (2014).
- [6] C. Gregory *et al.*, Nature **546**, 227 (2017).
- [7] S. Fajfer, J. F. Kamenik, I. Nišandžić, and J. Zupan, Phys. Rev. Lett. **109**, 161801 (2012).
- [8] S. L. Glashow, D. Guadagnoli, and K. Lane, Phys. Rev. Lett. **114**, 091801 (2015).
- [9] Y. Kuno and Y. Okada, Rev. Mod. Phys. **73**, 151 (2001).
- [10] S. Dell’Oro *et al.*, Adv. High Energy Phys.2016 (2016) 2162659.
- [11] D. A. Bryman *et al.*, Phys. Rev. Lett. **28**, 1469 (1972).
- [12] A. Badertscher *et al.*, Phys. Lett. B **79**, 371 (1978).
- [13] R. Abela *et al.*, Phys. Lett. B **95**, 318 (1980).
- [14] A. Badertscher *et al.*, Nucl. Phys. A **377**, 406 (1982).
- [15] S. Ahmad *et al.*, Phys. Rev. D **38**, 2102 (1988).
- [16] C. Dohmen *et al.*, Phys. Lett. B **317**, 631 (1993).
- [17] J. Kaulard *et al.*, Phys. Lett. B **422**, 334 (1998).
- [18] R. Appel *et al.*, Phys. Rev. Lett. **85**, 2877 (2000).
- [19] J. Batley *et al.*, Phys. Lett. B **697**, 107 (2011).
- [20] J. Batley *et al.*, Phys. Lett. B **769**, 67 (2017).
- [21] Phys. Lett. B **479**, 33 (2000).
- [22] M. Agostini *et al.* (GERDA Collaboration), Nature **544**, 47 (2017).
- [23] A. Gando *et al.* (KamLAND-Zen Collaboration), Phys. Rev. Lett. **117**, 082503 (2016).
- [24] J. M. Berryman, A. de Gouvêa, K. J. Kelly, and A. Kobach, Phys. Rev. D **95**, 115010 (2017).
- [25] T. Geib, A. Merle, and K. Zuber, Phys. Lett. B **764**, 157 (2017).
- [26] C. S. Chen, C. Q. Geng, and J. N. Ng, Phys. Rev. D **75**, 053004 (2007).
- [27] S. F. King, A. Merle, and L. Panizzi, J. High Energy Phys. **2014**, 124 (2014).
- [28] P. Pritimita, N. Dash, and S. Patra, Journal of High Energy Physics **2016**, 147 (2016).
- [29] Y. G. Cui *et al.*, KEK Report 2009-10.
- [30] R. Abramishvili *et al.*, KEK Report 2015-1.
- [31] L. Bartoszek *et al.* (Mu2e Collaboration), arXiv:1501.05241.
- [32] M. Wang *et al.*, Chinese Physics C **41**, 030003 (2017).
- [33] E. Borie and G. A. Rinker, Rev. Mod. Phys. **54**, 67 (1982).
- [34] Physics Reports **354**, 243 (2001).
- [35] T. Suzuki, D. F. Measday, and J. P. Roalsvig, Phys. Rev. C **35**, 2212 (1987).
- [36] H. Primakoff, Rev. Mod. Phys. **31**, 802 (1959).
- [37] M. Döbeli *et al.*, Phys. Rev. C **37**, 1633 (1988).
- [38] D. S. Armstrong *et al.*, Phys. Rev. C **46**, 1094 (1992).
- [39] P. C. Bergbusch *et al.*, Phys. Rev. C **59**, 2853 (1999).
- [40] P. Christillin, Nucl. Phys. A **362**, 391 (1981).
- [41] M. Gmitro, A. A. Ovchinnikova, and T. V. Teterova, Nucl. Phys. A **453**, 685 (1986).
- [42] S. Agostinelli *et al.*, Nucl. Instrum. Methods Phys. Res. A **506**, 250 (2003).